Supporting Information for:

High-Performance Concurrent Chemo-immuno-radiotherapy for the Treatment of Hematologic Cancer through Selective High-Affinity Ligand (SHAL) Antibody Mimic-Functionalized Doxorubicin-Encapsulated Nanoparticles

Kin Man Au,[1,2] *Rod Balhorn,*[3] *Monique C. Balhorn,*[3] *Steven I. Park,*[4,5]* *Andrew Z. Wang*[1,2]*

[1] Laboratory of Nano- and Translational Medicine, Carolina Center for Cancer Nanotechnology Excellence, Carolina Institute of Nanomedicine, University of North Carolina at Chapel Hill, Chapel Hill, NC 27599, USA.

[2] Department of Radiation Oncology, Lineberger Comprehensive Cancer Center, University of North Carolina at Chapel Hill, Chapel Hill, NC 27599, USA.

[3] SHAL Technologies, Inc., 15986 Mines Road, Livermore, CA 94550, USA.

[4] Lineberger Comprehensive Cancer Center, University of North Carolina at Chapel Hill, Chapel Hill, NC 27599, USA.

[5] Levine Cancer Institute, Atrium Health, Division of Hematology and Oncology, 100 Medical Park Dr, Suite 110, Concord, NC 28025, USA.

*Correspondence should be addressed to steven.park@carolinashealthcare.org (S.I.P.) or zawang@med.unc.edu (A.Z.W.).

SUPPORTING FIGURES

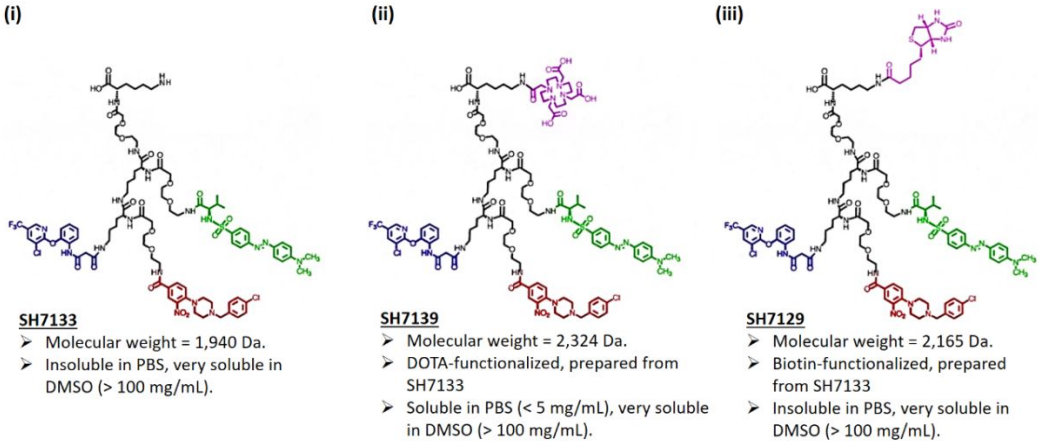

Figure S1. Chemical structures and water solubility of (i) SH7133 (primary amine-functionalized SHAL), (ii) SH7139 (DOTA-functionalized SHAL), and (iii) SH7129 (biotin-functionalized SHAL). SH7139 and SH7129 were prepared from SH7133. The synthesis, purification, and characterization of all SHALs were reported in references 21, 22, 29 and 58.

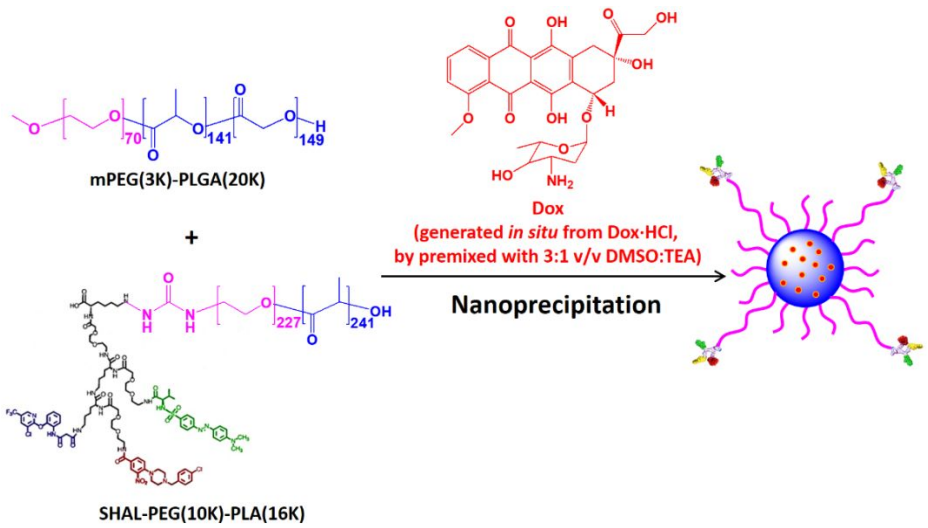

Figure S2. Synthesis of SHAL-functionalized Dox-encapsulated PEG-PLGA nanoparticles *via* nanoprecipitation. The building block of the PEG-PLGA NPs was PEG-PLGA. Hydrophilic Dox·HCl was converted to hydrophobic Dox *in situ* before the preparation of the NPs. The precipitation pH was about 9.0.

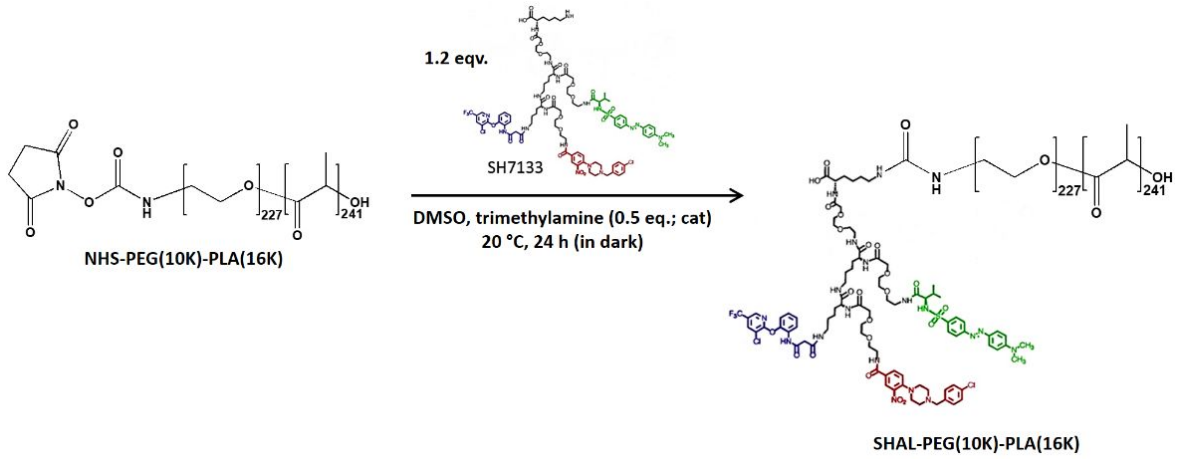

Figure S3. Synthesis of a SHAL-functionalized PEG-PLA diblock copolymer from amine-functionalized SHAL (SH7133) and a PLA(16K)-PEG(10K)-NHS ester.

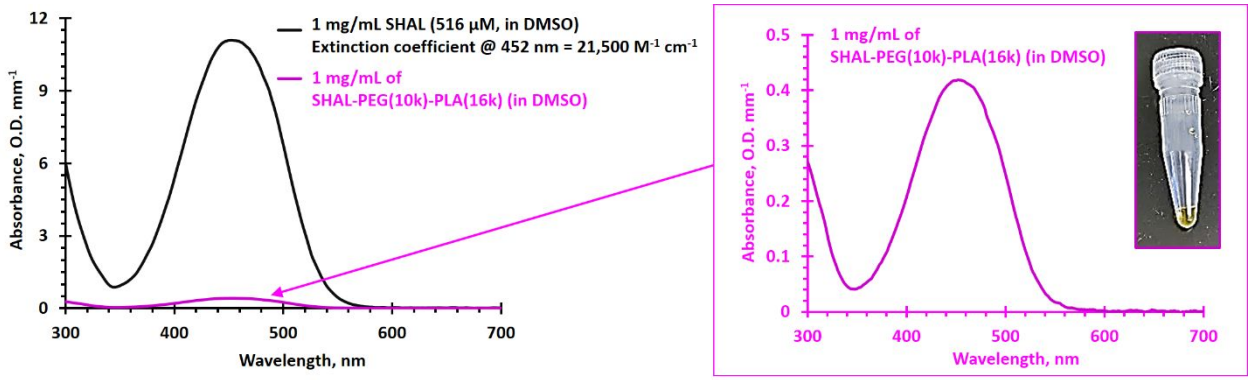

Figure S4. Ultraviolet-visible spectra of amine-functionalized SHAL (SH7133, 1 mg/mL in DMSO, 516 µM) and purified SHAL-functionalized PEG-PLA (1 mg/mL in DMSO). The extinction coefficient of SH7133 at 454 nm was 21,500 M^{-1} cm^{-1}. It was calculated that 52.7 mol% of the PEG-PLA was functionalized with SH7133 (conjugation efficiency ≈ 59%, since 90% of the PEG-PLA was functionalized with the NHS ester). The inset shows a digital image of the SHAL-functionalized PEG-PLA (1 mg/mL in DMSO).

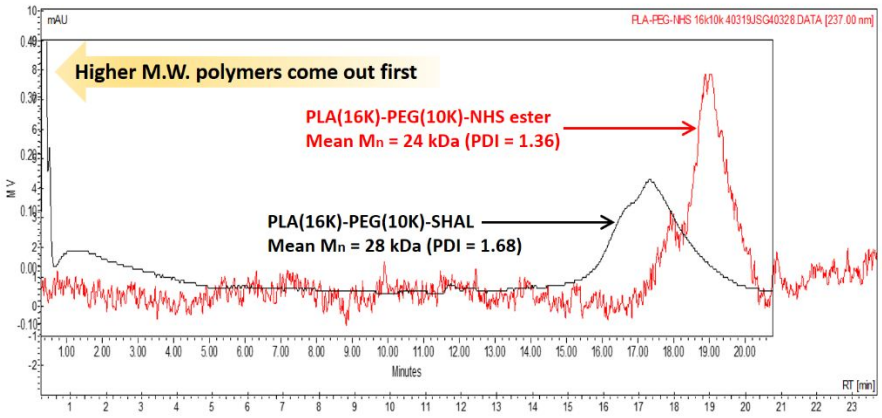

Figure S5. Tetrahydrofuran (THF) gel permeation chromatography (GPC) traces of the PLA(16K)-PEG(10K)-NHS ester and purified PLA(16K)-PEG(10K)-SHAL. The molecular weights of both polymers were calculated using Agilent PS2 polystyrene standards.

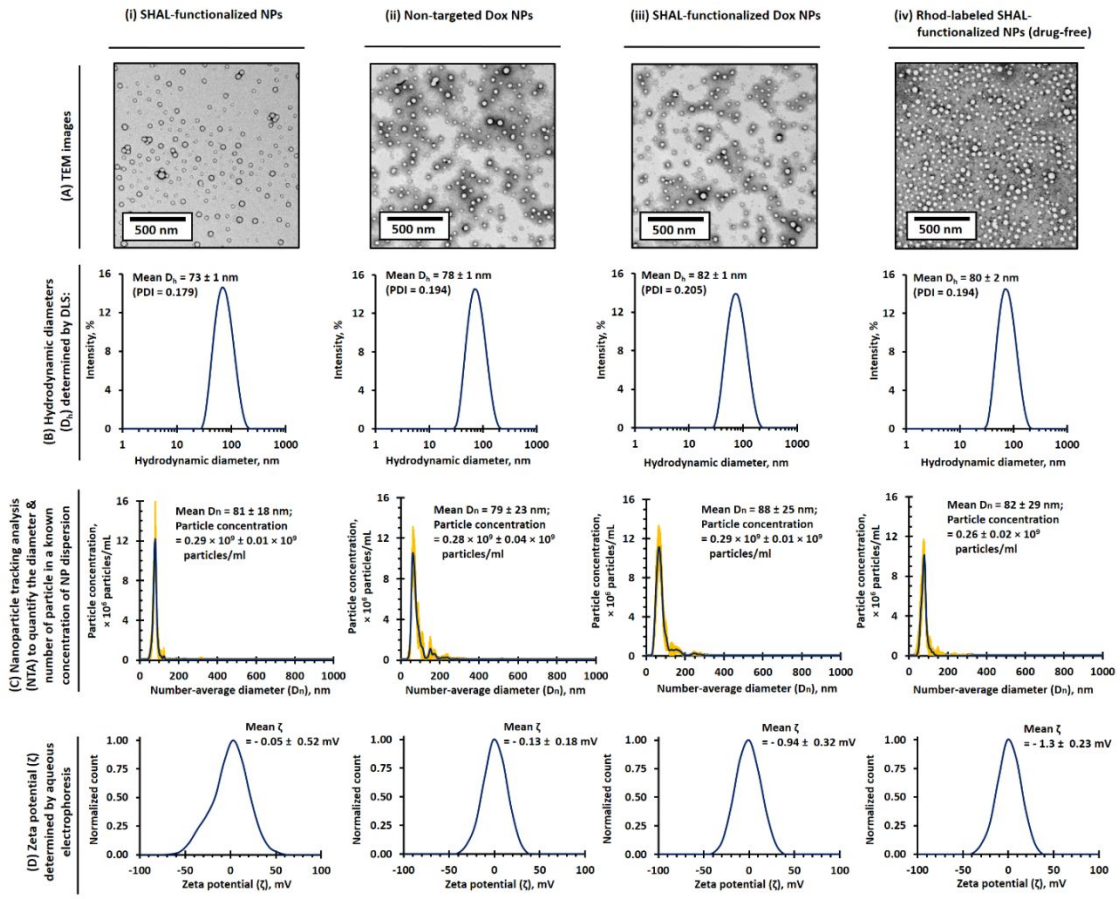

Figure S6. Characterization of (i) drug-free SHAL-functionalized NPs, (ii) non-targeted Dox-encapsulated PEG-PLGA NPs, (iii) SHAL-functionalized Dox-encapsulated NPs, and (iv) SHAL-functionalized Rhod-labeled PEG-PLGA NPs. (A) TEM images of non-targeted and SHAL-functionalized PEG-PLGA NPs. The number-average diameters of the PEG-PLGA NPs were 50–60 nm. (B) The plot of intensity-average diameters (also known as hydrodynamic diameters (D_h)) and their polydispersities (PDIs) of different PEG-PLGA NPs, as determined using the dynamic light scattering method. The mean D_h of most PEG-PLGA NPs were 70–85 nm, and the PDI was about 0.20. (C) The number-average diameter of different PEG-PLGA NPs as determined by the nanoparticle tracking analysis (NTA) method on NP dispersions. The mean D_n of different PEG-PLGA NPs was about 80 nm. (D) The plot of the zeta potentials (ζ) of different PEG-PLGA NPs dispersed in 0.1 M PBS determined by an aqueous electrophoresis method.

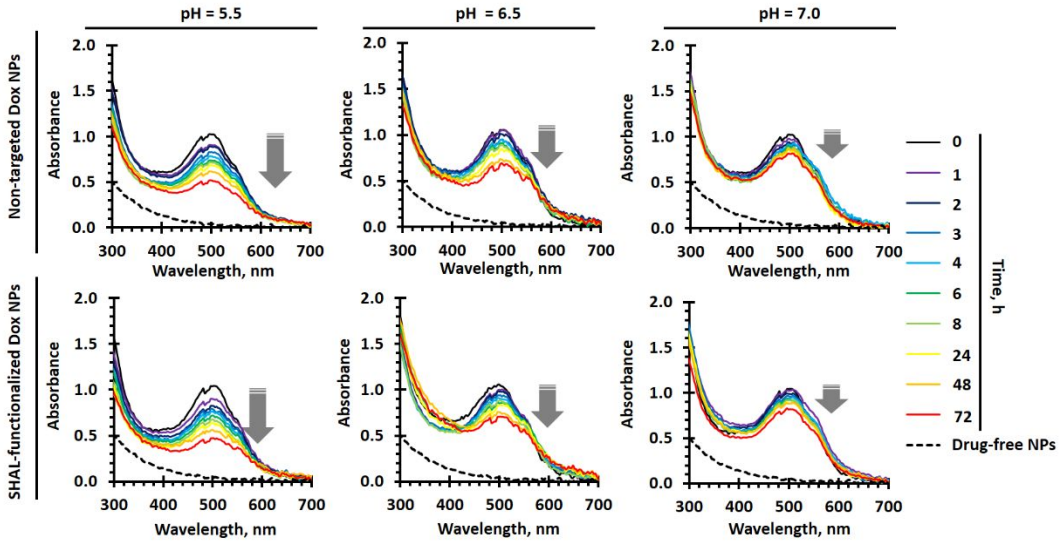

Figure S7. Drug release kinetics at neutral (pH 7.0) and different mild acidic (either 6.5 or pH 5.5) conditions. Averaged time-dependent ultraviolet-visible spectra of (i) non-targeted Dox NPs and (ii) SHAL-functionalized Dox NPs after incubation in a large excess of 1X PBS at pH 5.5, 6.5 or 7.0 at 37 °C. The concentrations of both NPs were 2 mg/mL. The drug-encapsulation efficiencies of the non-targeted Dox NPs and SHAL-functionalized Dox NPs were 56.7 ± 1.0% (i.e., 1 mg NPs contains 28.4 µg encapsulated Dox) and 57.8 ± 1.1% (i.e., 1 mg NPs contains 28.9 µg encapsulated Dox), respectively. (n = 3).

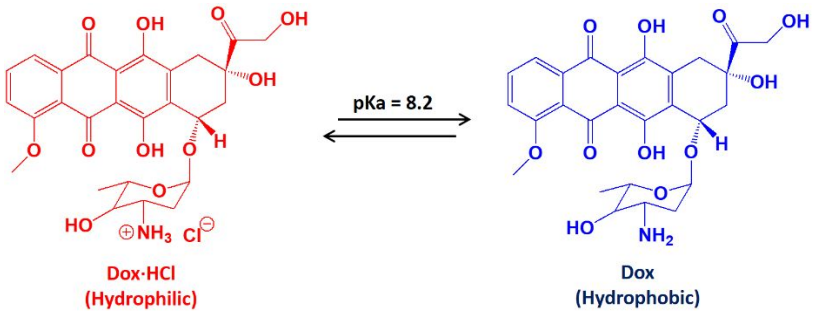

Figure S8. Chemical structures and solubility of doxorubicin (Dox) at different pHs. The Figure was adapted with modification from reference 34.

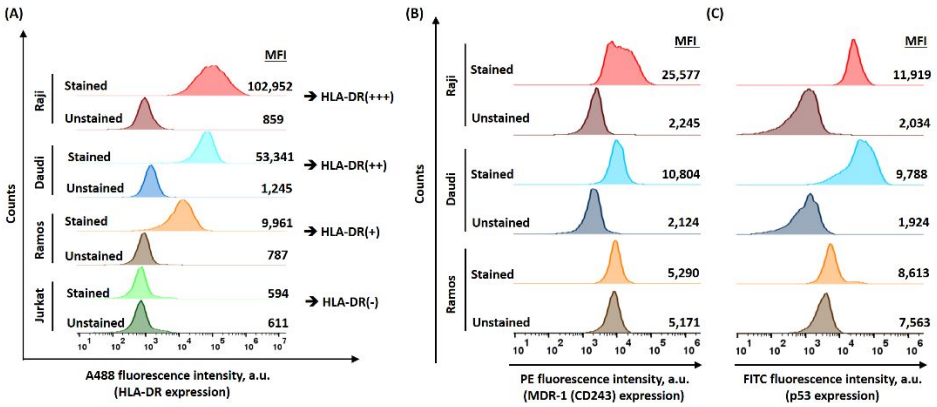

Figure S9. (A) HLA-DR expressions of 4 well-established lymphoma cell lines. (B and C) MDR-1 and p53 expressions of 3 different HLA-DR-expressed Ramos, Daudi and Raji cells. The amounts of HLA-DR, MDR-1, and intracellular p53 expressions were quantified by FACS method after staining the cells with an A488-labeled anti-human HLA-DR antibody (BioLegend, Clone L243), PE-labeled anti-human CD243 antibody (BioLegend, Clone: 4E3.16) and FITC-labeled anti-human p53 antibody (BioLegend, Clone DO-7), respectively.

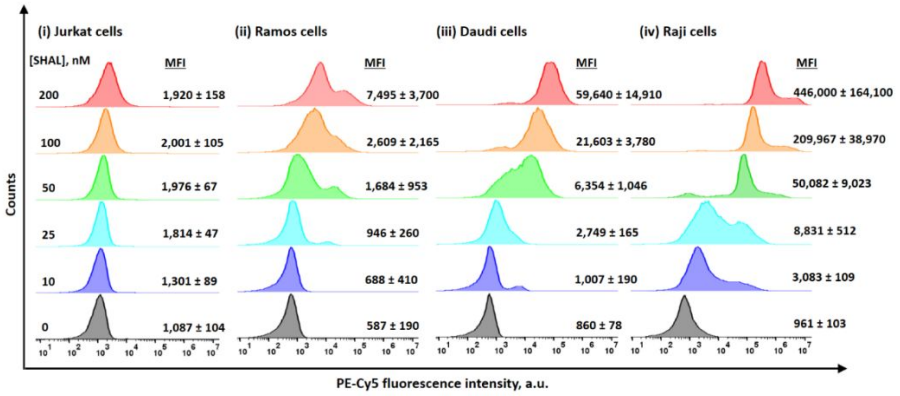

Figure S10. Binding affinities of biotin-functionalized SHAL (SH7129) in different lymphoma cell lines with different HLA-DR antigen expressions. Representative FACS histograms of (i) Jurkat, (ii) Ramos, (iii) Daudi, and (iv) Raji cells after staining with different concentrations (0–200 nM) of biotin-functionalized SHAL and detecting the bound SHAL using streptavidin-PE-Cy5. The cells were pre-blocked with a biotin-streptavidin blocking agent before the binding study to prevent non-specific binding. (n = 3)

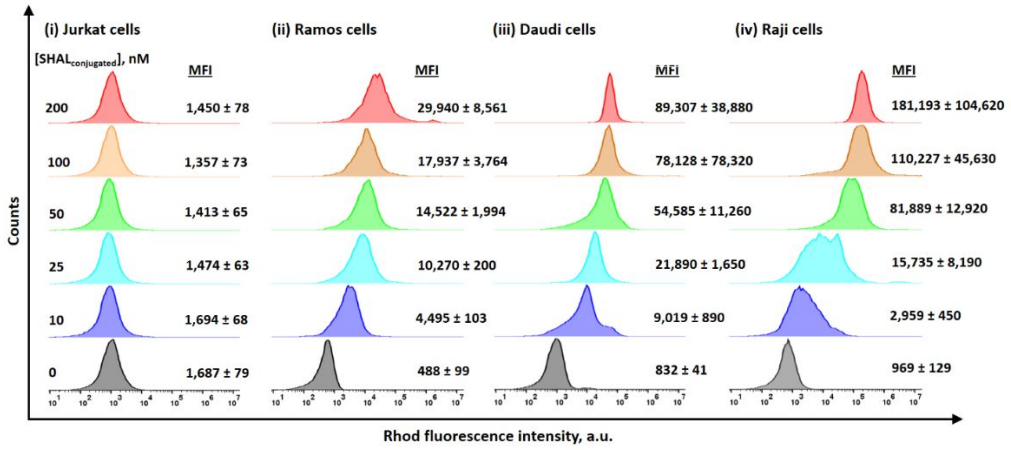

Figure S11. Binding affinities of SHAL-functionalized Rhod-labeled NPs in different lymphoma cell lines with different HLA-DR antigen expressions. Representative FACS histograms of (i) Jurkat, (ii) Ramos, (iii) Daudi, and (iv) Raji cells after staining with different concentrations of Rhod-labeled SHAL-functionalized NPs (contained 0–200 nM of conjugated SHAL. (n = 3)

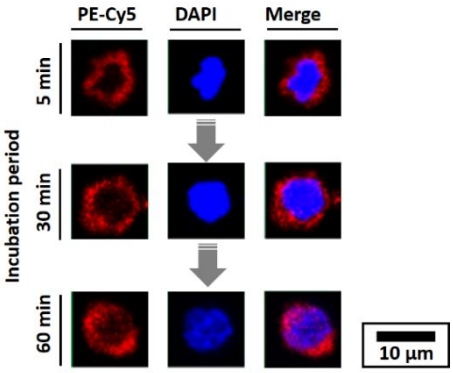

Figure S12. Time-dependent CLSM images of Raji cells after staining with biotin-functionalized SHAL (SH7129) (with attached PE-Cy5-functionalized streptavidin to enable visualization of the complex) and subsequent incubation at physiological conditions for 5–60 min. Red is PE-Cy5 staining of SH7129 bound to PE-Cy5-streptavidin. Blue is DAPI staining of the nucleus.

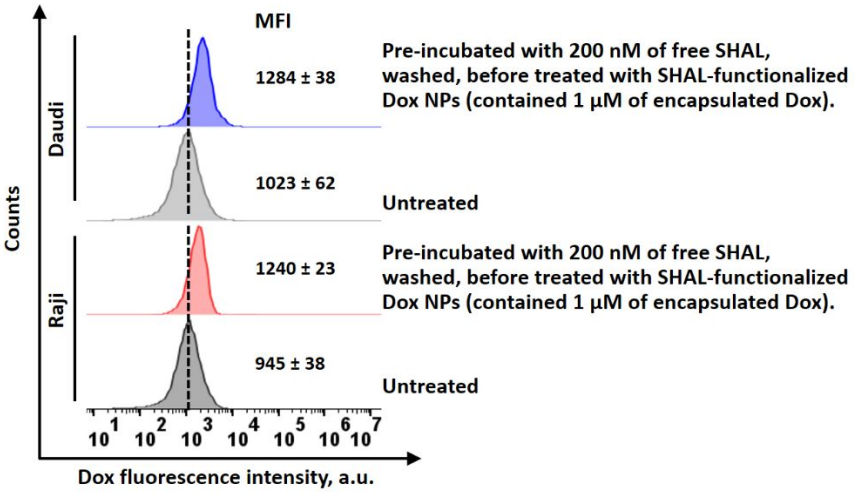

Figure S13. *In vitro* uptake of SHAL-functionalized Dox NPs (contained 1 µM of encapsulated Dox) by free-SHAL (hydrophilic DOTA-functionalized SHAL, SH7139)-pretreated Daudi and Raji cells, as quantifued by FACS method.

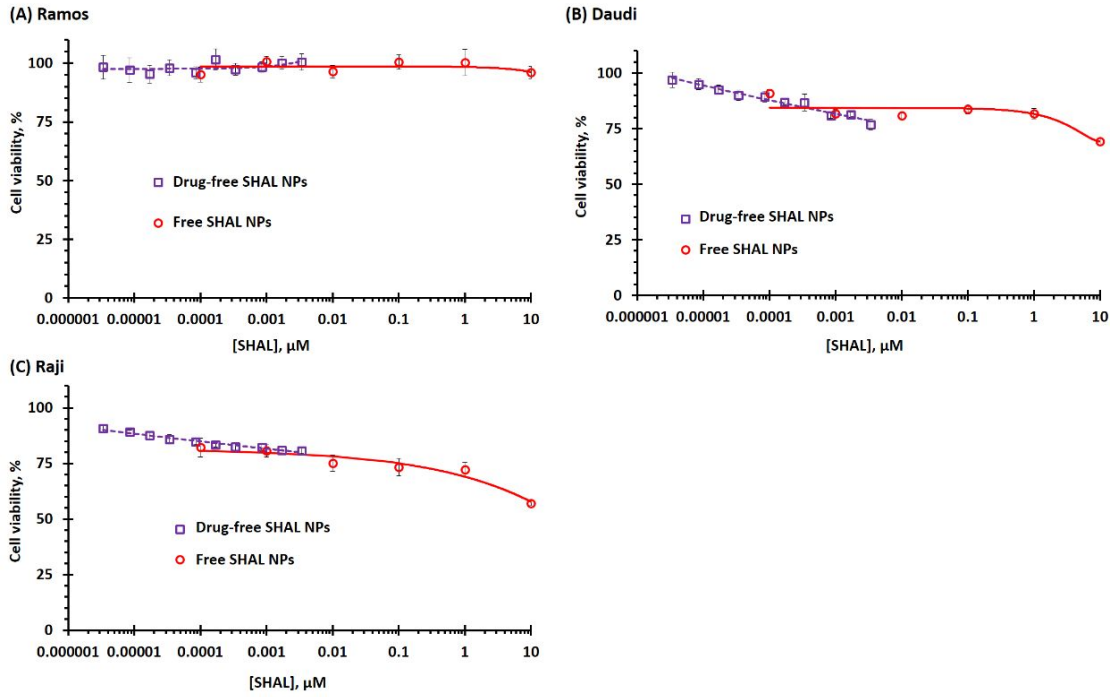

Figure S14. *In vitro* toxicities of free SHAL (DOTA-functionalized SHAL, SH7139) and drug-free SHAL-functionalized NPs in (A) Ramos, (B) Daudi, and (C) Raji cells. The cell viabilities were quantified after treatment using an MTS assay. The toxicities of free SHAL and SHAL-functionalized NPs in all three cell lines were well above 10 µM. (n = 8 per group).

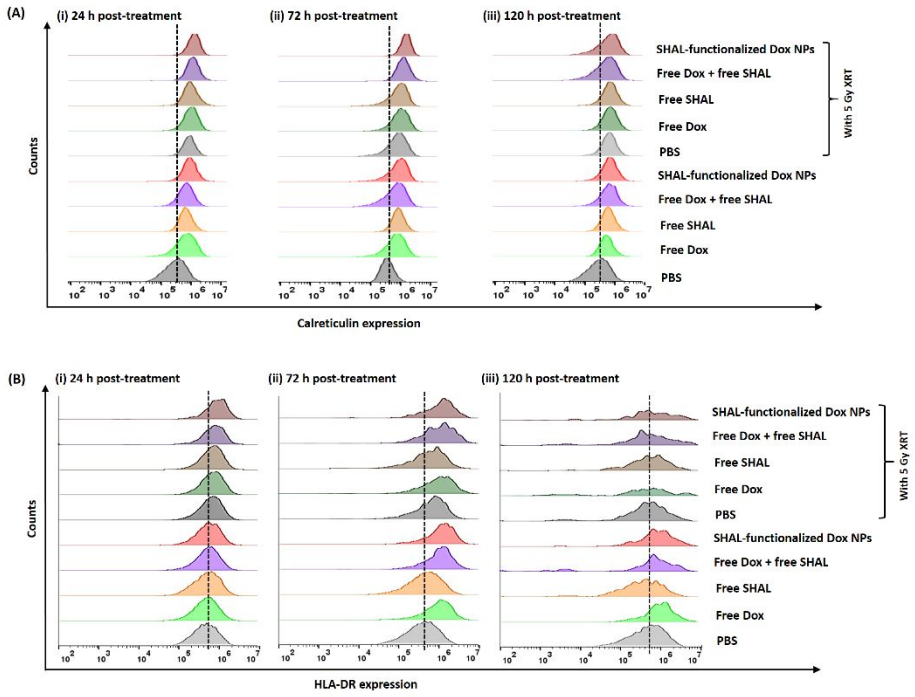

Figure S15. (A) Representative flow histograms of A488-labeled anti-calreticulin-stained Raji cells at 1, 3, and 5 days after treatment with IC_{25} of Dox (either free or encapsulated Dox), with or without 5 Gy X-ray irradiation (which occurs 24 h after the initial drug treatment). (B) Representative flow histograms of A488-labeled anti-HLA-DR-stained Raji cells at 1, 3, and 5 days after treatment with IC_{25} of Dox (either free or encapsulated Dox), with or without 5 Gy X-ray irradiation (which occurs 24 h after the initial drug treatment).

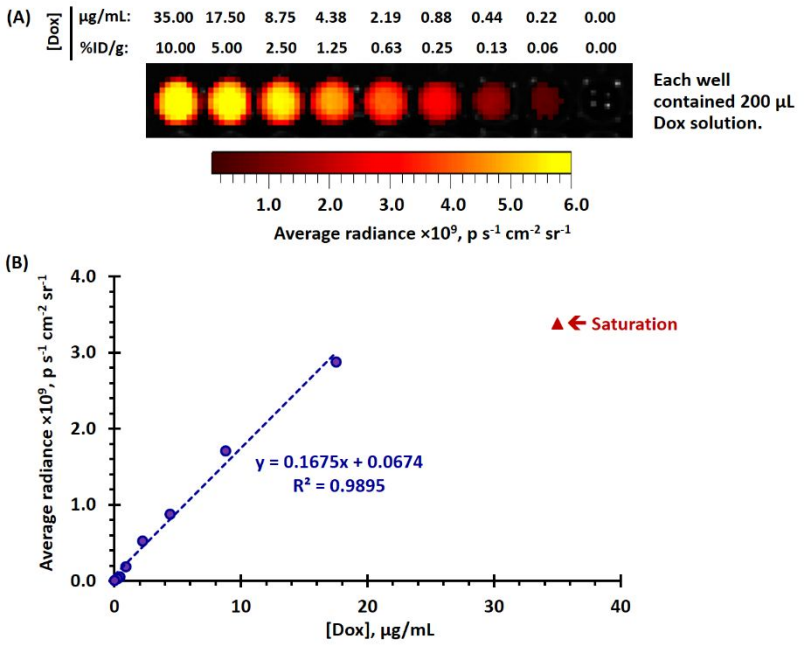

Figure S16. Quantification of Dox *via* the IVIS Kinetic imaging system. (A) Fluorescence image of different concentrations of Dox (dissolved in 1X PBS). The image was recorded *via* an IVIS Kinetic imaging system. The *ex vivo* fluorescence image was recorded using a DsRed emission filter (λ_{em} = 575–650 nm) upon excitation at 465 ± 15 nm. (B) The plot of the average radiances of different concentrations of Dox solutions. The average radiances increase linearly with Dox concentrations up to 17.5 µg/mL.

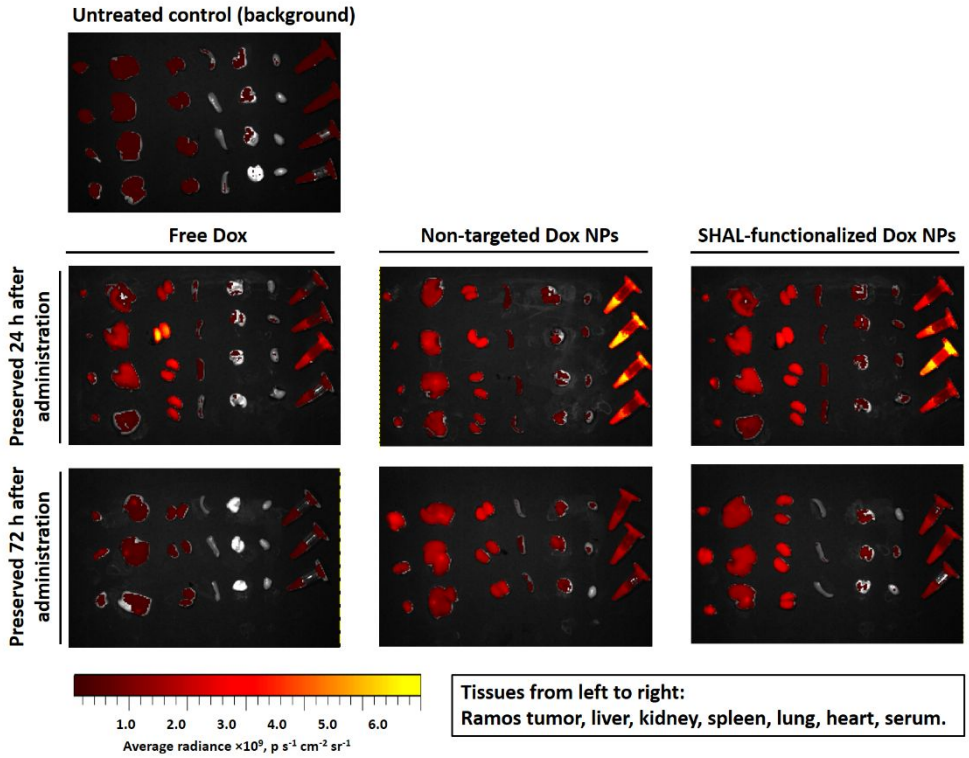

Figure S17. Biodistribution of free or encapsulated Dox in Ramos xenograft tumor-bearing mice. *Ex vivo* fluorescence images of Ramos xenograft tumors, key organs (liver, kidney, spleen, lung, and heart), and serum harvested from Ramos xenograft tumor-bearing mice 24 or 72 h after tail vein i.v. injection of 3.5 mg/kg of free or encapsulated Dox. The Ramos xenograft tumor, liver, kidney, spleen, lung, heart, and serum were preserved from non-treated mice as a control. The *ex vivo* fluorescence images were recorded through a DsRed emission filter (λ_{em} = 575–650 nm) upon excitation at 465 ± 15 nm (n = 4 per group for all experimental and control groups, except n = 3 for the treatment groups preserved 72 h after the i.v. injection).

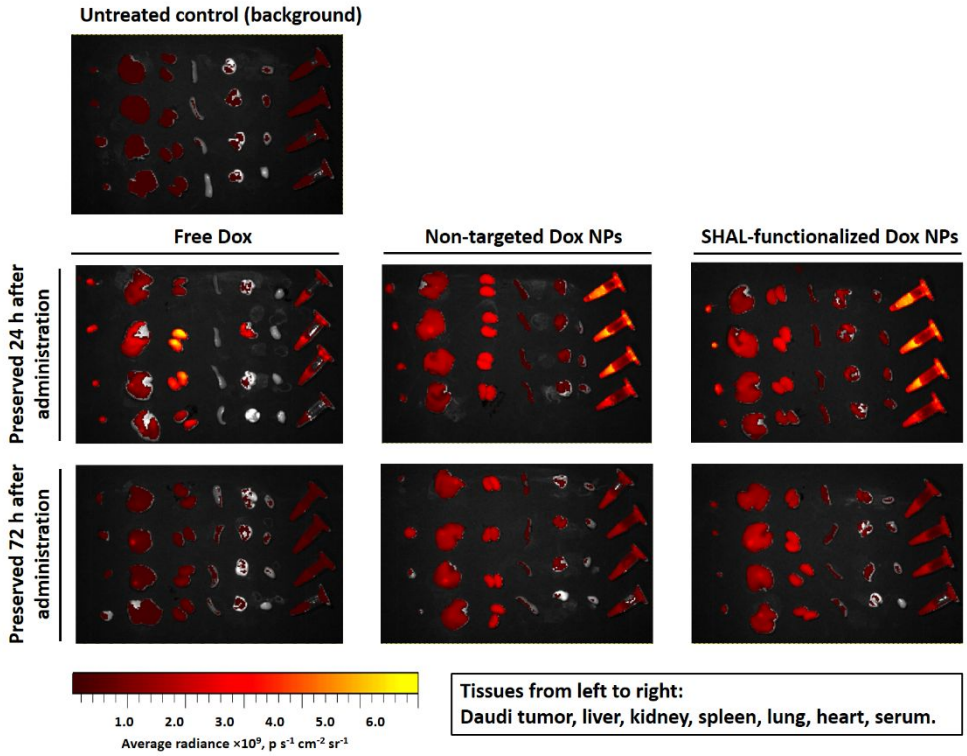

Figure S18. Biodistribution of free or encapsulated Dox in Daudi xenograft tumor-bearing mice. *Ex vivo* fluorescence images of Daudi xenograft tumor, key organs (liver, kidney, spleen, lung, and heart), and serum harvested from Daudi xenograft tumor-bearing mice 24 or 72 h after tail vein i.v. injection of 3.5 mg/kg of free or encapsulated Dox. The Daudi xenograft tumor, liver, kidney, spleen, lung, heart, and serum were preserved from non-treated mice as a control. The *ex vivo* fluorescence images were recorded through a DsRed emission filter (λ_{em} = 575–650 nm) upon excitation at 465 ± 15 nm. (n = 4 per group)

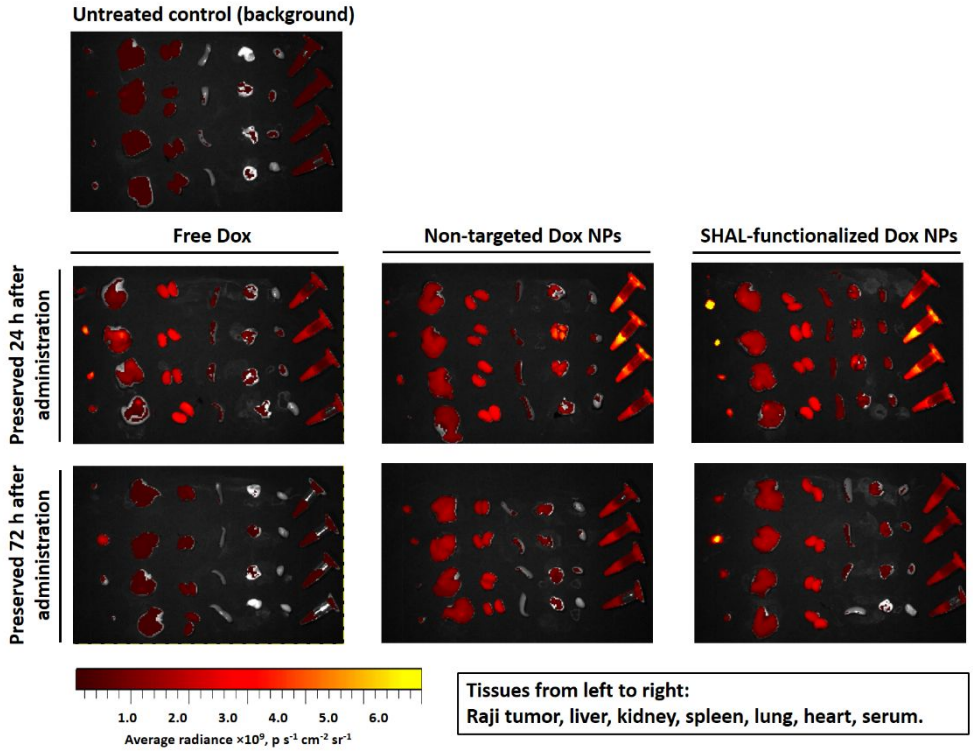

Figure S19. Biodistribution of free or encapsulated Dox in Raji xenograft tumor-bearing mice. *Ex vivo* fluorescence images of the Raji xenograft tumor, key organs (liver, kidney, spleen, lung, and heart), and serum harvested from Raji xenograft tumor-bearing mice 24 or 72 h after the tail vein i.v. injection of 3.5 mg/kg of free or encapsulated Dox. The Raji xenograft tumor, liver, kidney, spleen, lung, heart, and serum were preserved from non-treated mice as a control. The *ex vivo* fluorescence images were recorded using a DsRed emission filter (λ_{em} = 575–650 nm) upon excitation at 465 ± 15 nm. (n = 4 per group)

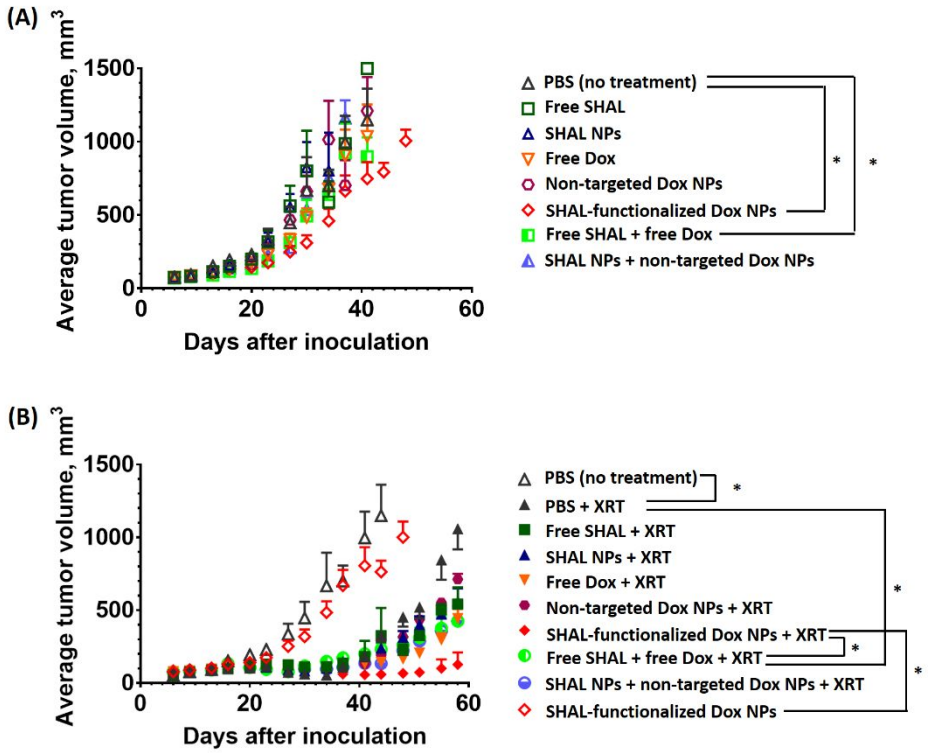

Figure S20. *In vivo* anticancer activities of Dox and Dox nanoformulations for chemo-immunotherapy and concurrent CIRT in the Daudi xenograft tumor model. (A) Averaged tumor growth curves of mice in the non-treatment control group and in different treatment groups that received treatment with small molecule Dox or different Dox nanoformulations. (B) Averaged tumor growth curves of mice in the non-treatment control group and different treatment groups that received treatment with small molecule Dox or different Dox nanoformulations. Mice in the concurrent CIRT groups received 5 Gy XRT 24 h after each i.v. administration of therapeutics. (n = 7 or 8; * denotes $p < 0.05$, i.e., statistically significant; n.s. denotes $p > 0.05$, i.e., statistically insignificant).

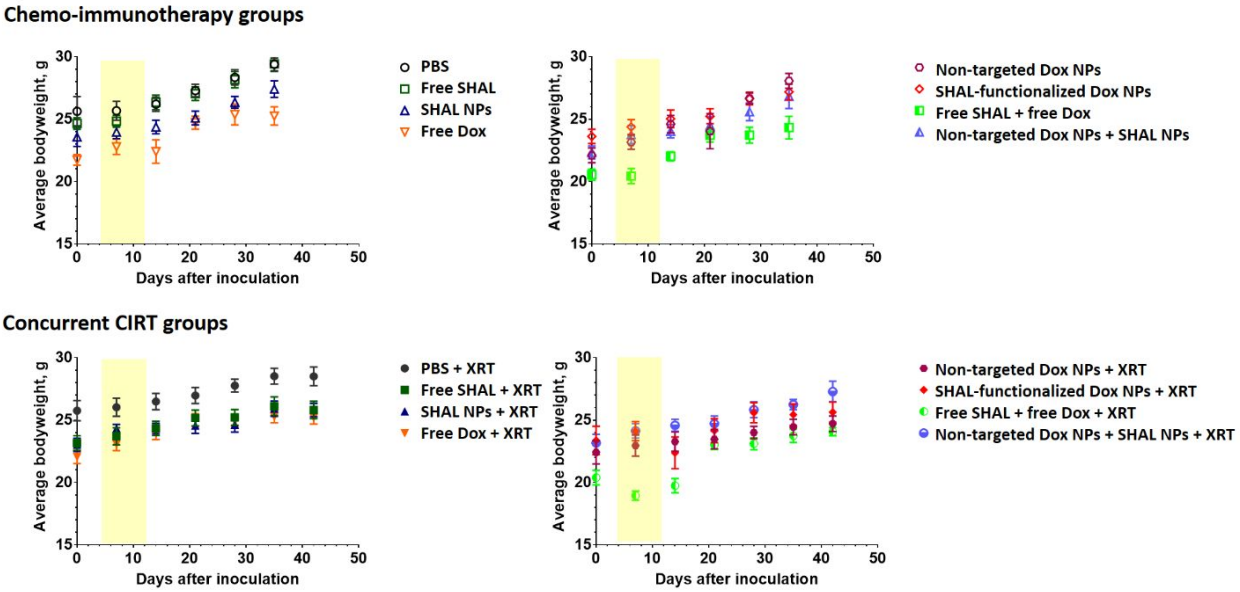

Figure S21. The average body weight of Daudi xenograft tumor-bearing mice after receiving different treatments. The yellow highlighted regions show the treatment period. (n = 7 or 8)

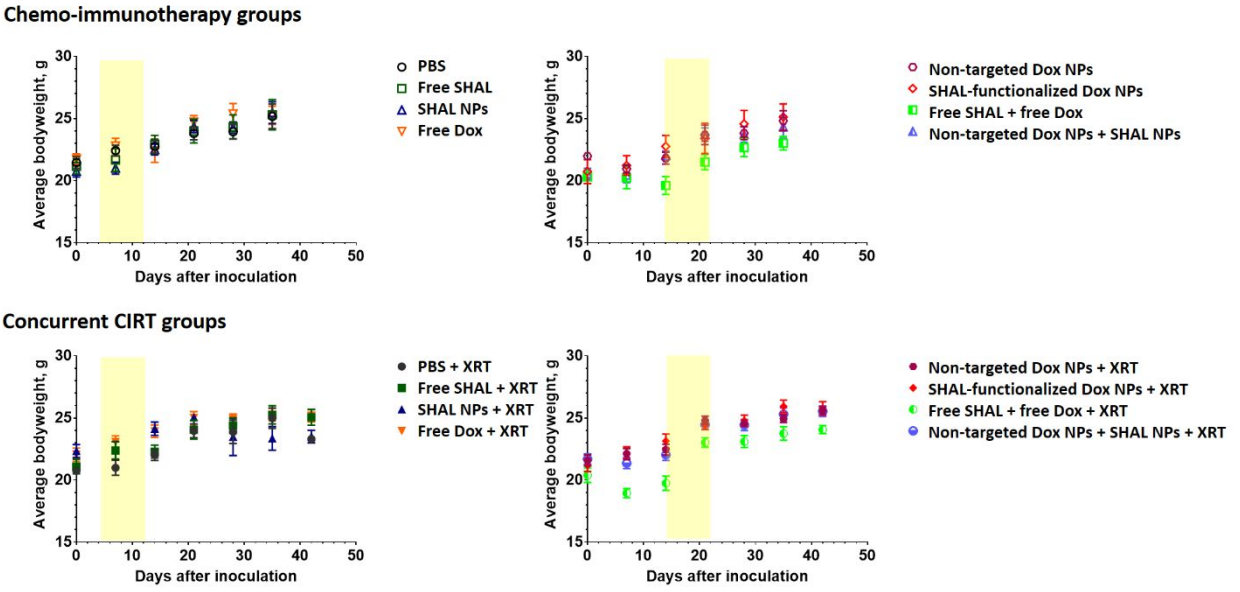

Figure S22. Average body weight of Raji xenograft tumor-bearing mice after receiving different treatments. Mice in the concurrent CIRT groups were given 5 Gy XRT 24 h after each i.v. administration of therapeutics. The yellow highlighted regions indicate the treatment period. (n = 6 or 7)

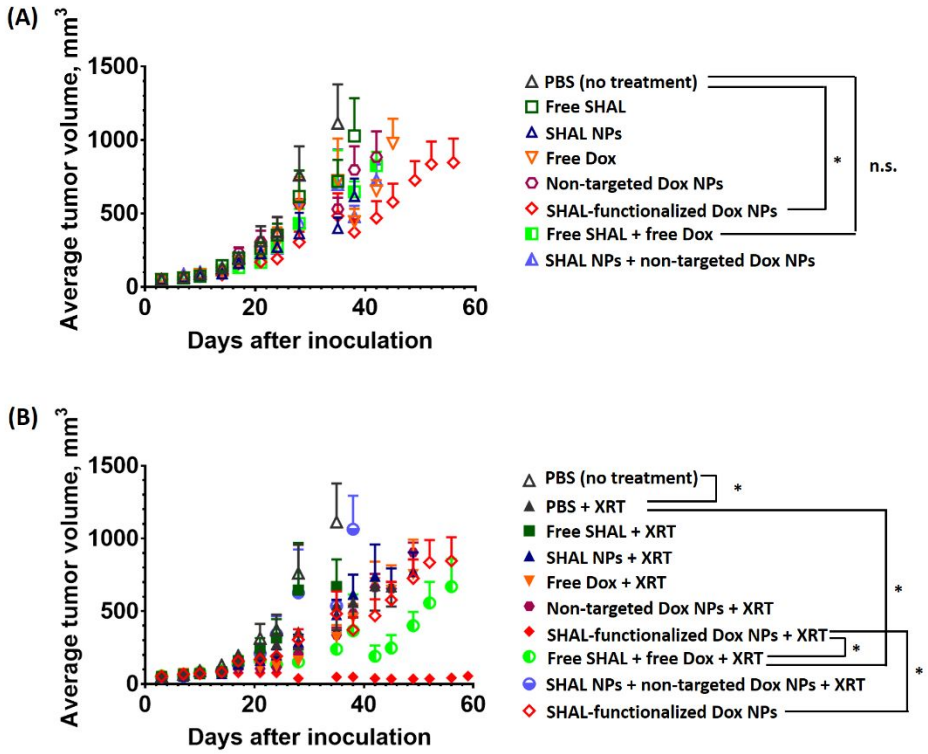

Figure S23. *In vivo* anticancer activities of Dox and Dox nanoformulations for chemo-immunotherapy and concurrent CIRT in the Raji xenograft tumor model. (A) The averaged tumor growth curves of mice in the non-treatment control group and different treatment groups receiving treatment with small molecule Dox or Dox nanoformulations. (B) Averaged tumor growth curves of mice in the non-treatment control group and in different treatment groups that received treatment with small molecule Dox or Dox nanoformulations. Mice in the concurrent CIRT groups received 5 Gy XRT 24 h after each i.v. administration of therapeutics (n = 6 or 7; * denotes $p < 0.05$, i.e., statistically significant; n.s. denotes $p > 0.05$, i.e., statistically insignificant).

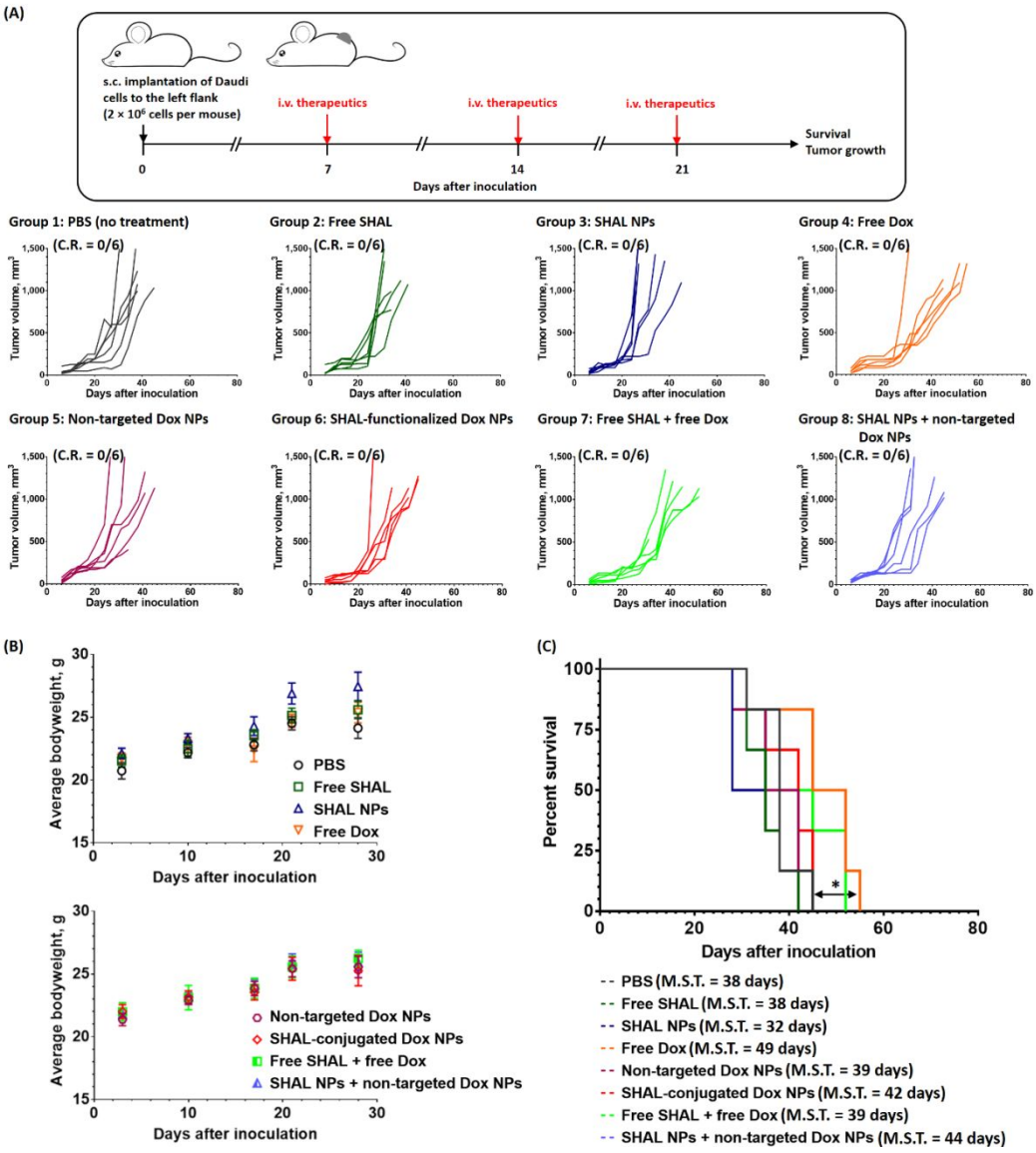

Figure S24. *In vivo* anticancer activities of free Dox and different Dox nanoformulations for chemo-immunotherapy in the Daudi xenograft tumor model with a less intense treatment schedule (i.e., a one week rest period between treatments). (A) The treatment schedule and tumor growth curve of individual mice in the control and treatment groups. Treatment doses were 3 × 3.5 mg/kg of free/encapsulated Dox and/or 3 × 5 μg/kg of free/conjugated SHAL. (B) The average bodyweight of mice in different control and treatment groups recorded after tumor inoculation. (C) Kaplan-Meier survival curves of mice in the non-treatment group and chemo-immunotherapy groups (n = 6 per group; * denotes $p < 0.05$, i.e., statistically significant).

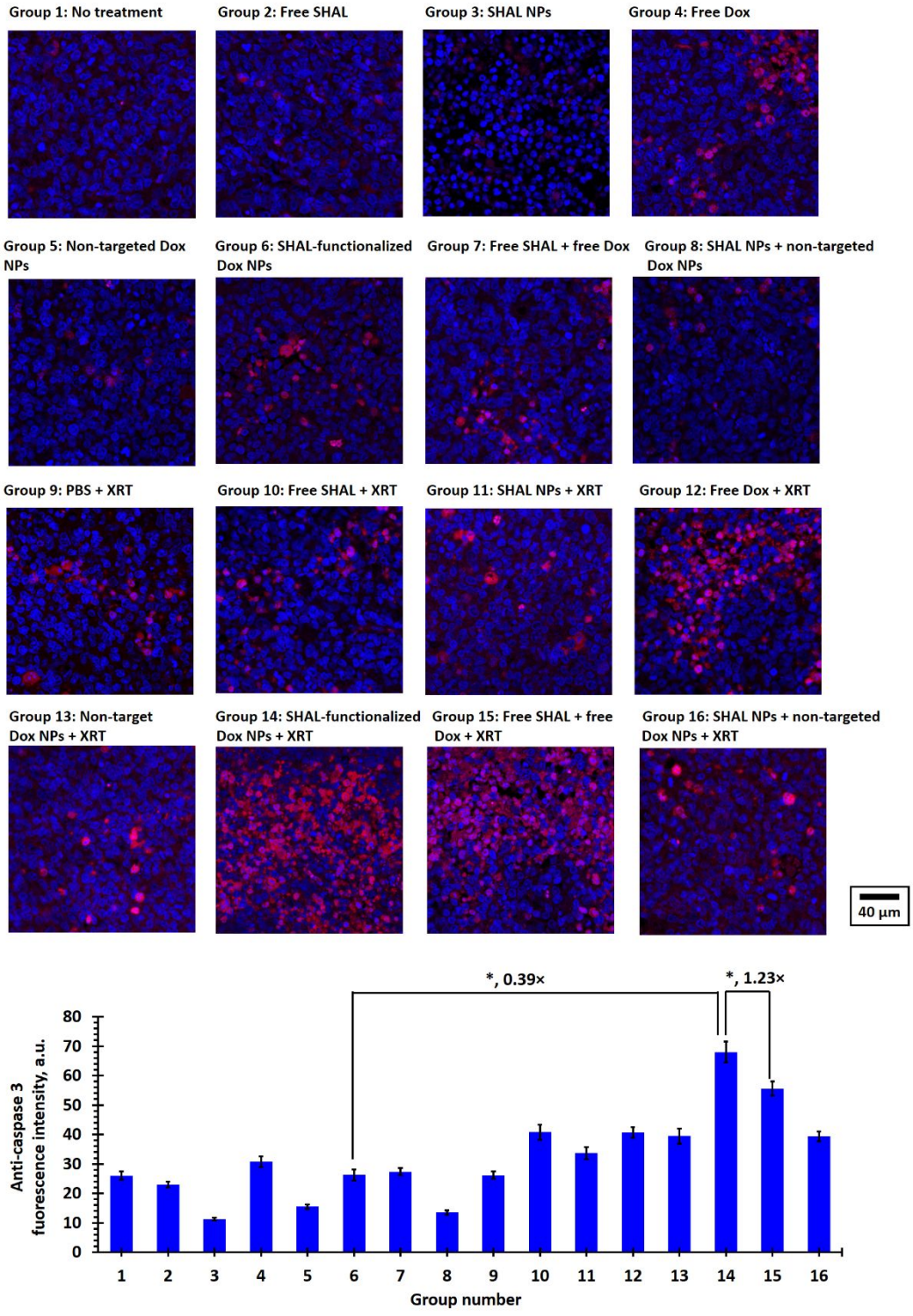

Figure S25. Representative CLSM images of anti-caspase 3-stained Raji tumor sections preserved 3 days after different treatments. All nuclei were stained with DAPI (blue fluorescence). The strong red fluorescence were caspase 3-positive cells. [n = 3 per group; * denotes $p < 0.05$, i.e., statistically significant.]

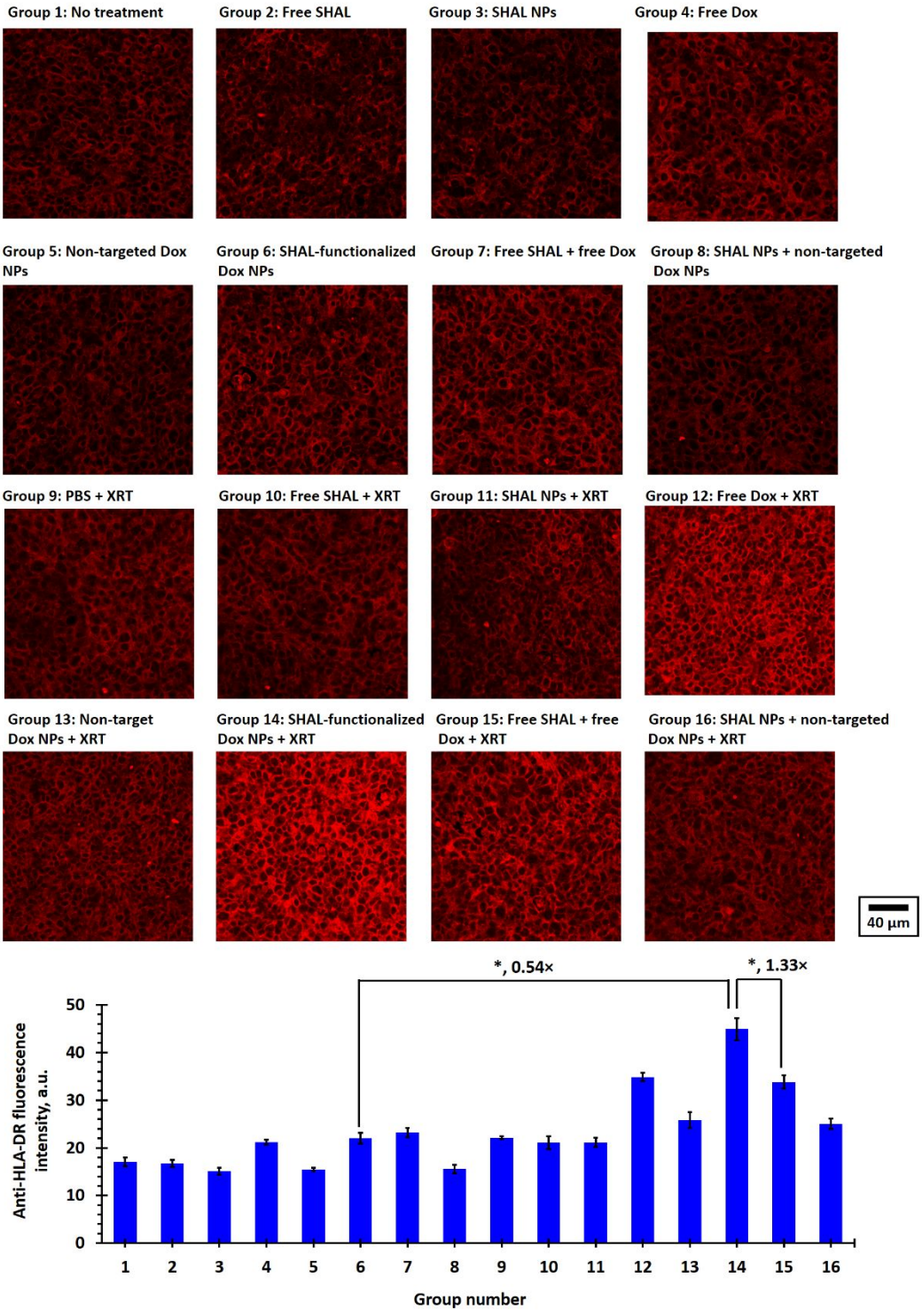

Figure S26. Representative CLSM images of anti-HLA-DR-stained Raji tumor sections preserved 3 days after different treatments. The fluorescence intensity proportional to the HLA-DR expression of the treated cancer cells. [n = 3 per group; * denotes $p < 0.05$, i.e., statistically significant.]

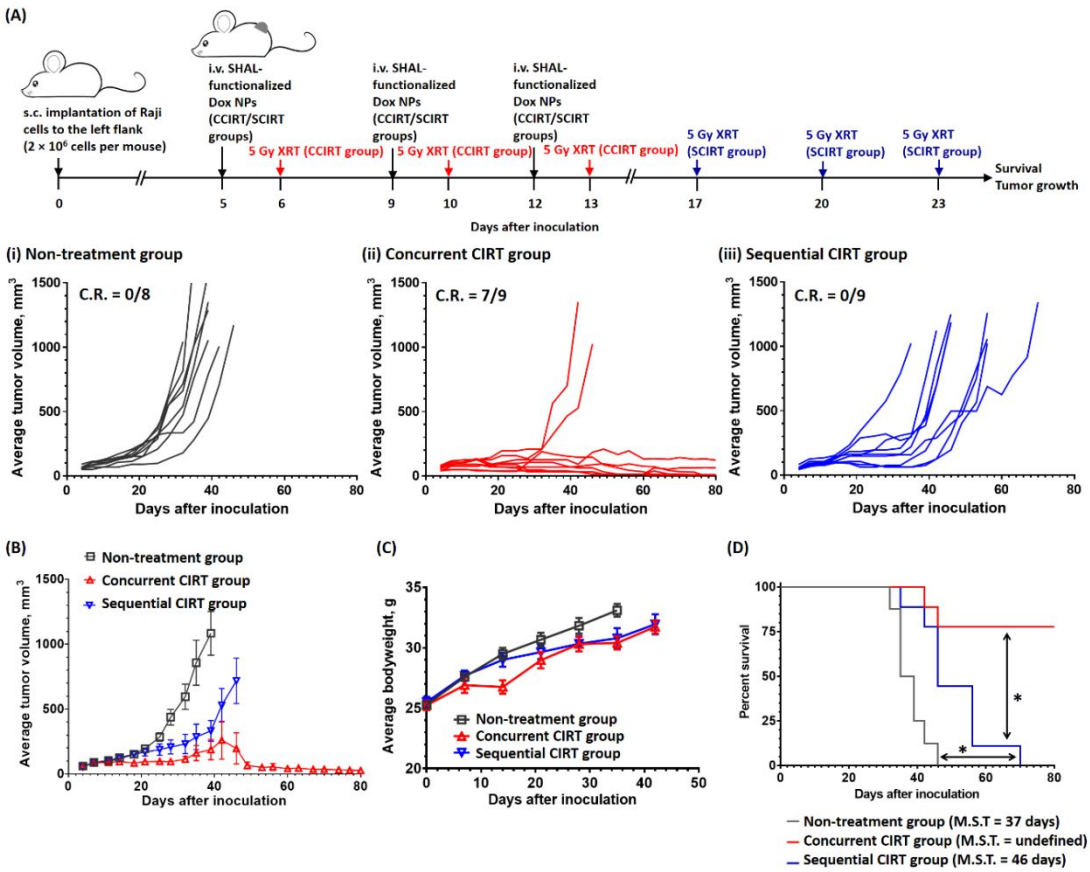

Figure S27. *In vivo* anticancer activities of SHAL-functionalized Dox NPs in a Raji xenograft tumor model administrated using different treatment schedules. (A) The treatment schedule and tumor growth curve of individual mice in the control and treatment groups. Treatment doses were 3 × 3.5 mg/kg of encapsulated Dox plus 3 × 5 μg/kg of conjugated SHAL. (B) Average tumor growth curves of mice in the non-treatment, concurrent CIRT and sequential CIRT groups. (C) The average bodyweight of mice in different control and treatment groups recorded after tumor inoculation. (D) Kaplan-Meier survival curves of mice in the non-treatment group and chemo-immunotherapy groups (n = 6 per group; * denotes $p < 0.05$, i.e., statistically significant).

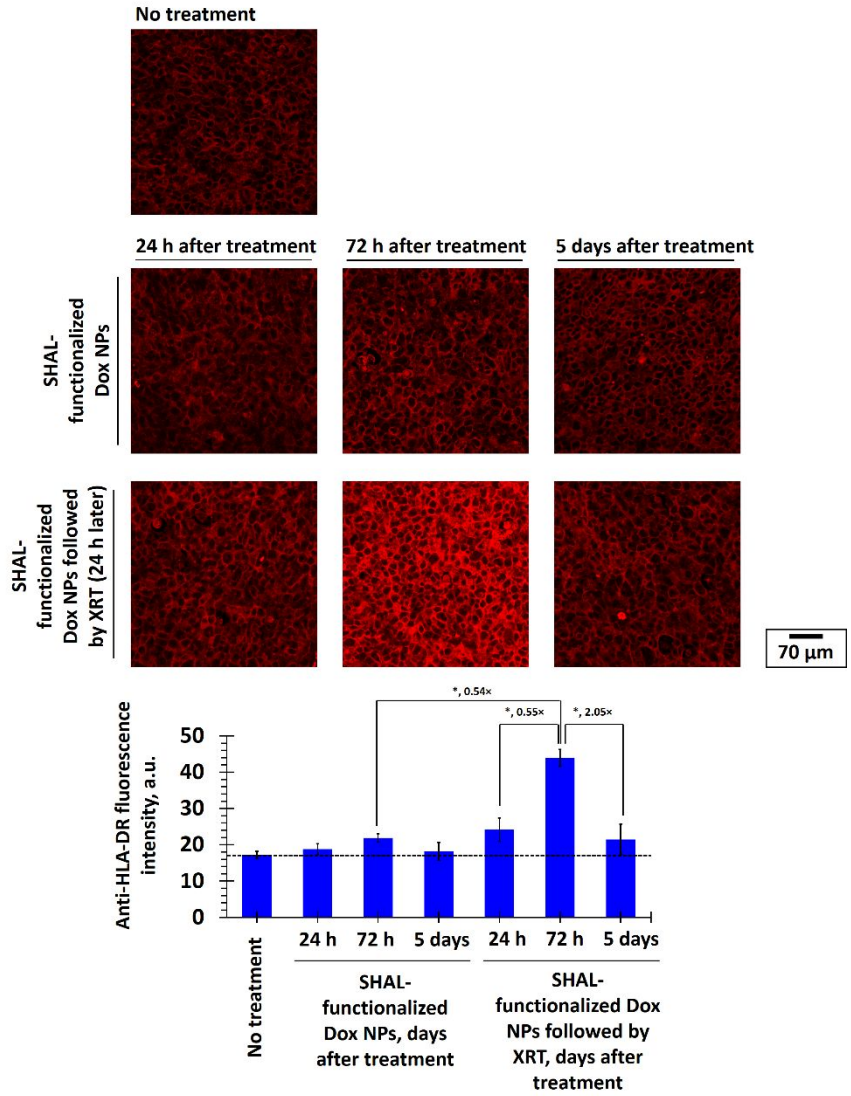

Figure S28. Representative CLSM images of anti-HLA-DR-stained Raji tumor sections preserved 24 h, 72 h and 5 days after the treatment with SHAL-functionalized Dox NPs (with and without 5 Gy XRT 24 h after the administration of SHAL-functionalized Dox NPs). The fluorescence intensity proportional to the HLA-DR expression of the treated cancer cells. [n = 3 per group; * denotes $p < 0.05$, i.e., statistically significant.]

SUPPORTING TABLES

	Reference range	PBS (control)	Free SHAL	Drug-free SHAL NPs	Free Dox	Non-targeted Dox NPs	SHAL-functionalized Dox NPs	Drug-free SHAL NPs + non-targeted Dox NPs	Free SHAL + free Dox	Drug-free mPEG-PLGA NPs
RBC, M/uL	8.9 ± 1.4	9.5 ± 0.5	9.1 ± 0.3	9.6 ± 0.2	9.3 ± 0.3	8.9 ± 0.3	8.9 ± 0.2	9.2 ± 0.1	9.3 ± 0.1	9.5 ± 0.3
HGB, g/dL	14.7 ± 2.2	15.8 ± 0.8	14.8 ± 0.4	15.6 ± 0.4	15.3 ± 0.3	14.7 ± 0.2	15.1 ± 0.5	14.9 ± 0.2	15.0 ± 0.2	15.4 ± 0.3
MCHC, g/dL	29.5 ± 2.8	30.7 ± 0.4	31.3 ± 0.2	30.5 ± 0.2	30.7 ± 0.1	31.2 ± 0.3	31.1 ± 0.1	31.8 ± 0.5	31.2 ± 0.3	30.7 ± 0.2
RET#, K/uL	338.3 ± 140.5	478.9 ± 68.4	394.4 ± 17.0	318.1 ± 46.6	39.7 ± 6.7 *	261.5 ± 75.3	254.2 ± 56.4	258.6 ± 32.4	52.4 ± 22.9 *	369.7 ± 48.8
PLT, K/uL	1538.9 ± 4006	805.8 ± 23.1	587.75 ± 82.1	656.4 ± 121.7	729.5 ± 169.7	728.2 ± 38.2	953.0 ± 75.4	780.8 ± 52.5	806.0 ± 28.7	799.4 ± 20.0
WBC, K/uL	3.8 ± 0.8	5.8 ± 1.3	6.4 ± 1.0	4.8 ± 0.8	5.2 ± 1.0	5.2 ± 0.4	5.0 ± 1.3	4.0 ± 0.6	5.7 ± 0.9	5.3 ± 0.4
NEUT#, K/uL	0.90 ± 0.40	0.82 ± 0.13	0.67 ± 0.15	0.50 ± 0.08	0.44 ± 0.05	0.64 ± 0.16	0.55 ± 0.04	0.46 ± 0.07	0.41 ± 0.05	0.66 ± 0.15
LYMPH#, K/uL	6.7 ± 2.2	7.1 ±1.2	8.1 ± 0.9	6.2 ± 0.8	3.2 ± 0.7 *	6.3 ± 0.4	7.2 ± 1.1	6.5 ± 0.5	3.5 ± 0.4 *	6.8 ± 0.3
MONO#, K/uL	0.10 ± 0.0	0.16 ± 0.03	0.28 ± 0.11	0.16 ± 0.01	0.48 ± 0.14	0.37 ± 0.08	0.22 ± 0.06	0.21 ± 0.2	0.19 ± 0.01	0.19 ± 0.05
EO#, K/uL	0.20 ± 0.20	0.08 ± 0.02	0.09 ± 0.02	0.11 ± 0.03	0.12 ± 0.02	0.09 ± 0.01	0.06 ± 0.01	0.07 ± 0.01	0.10 ± 0.02	0.08 ± 0.02
BASO#, K/uL	0.040 ± 0.050	0.006 ± 0.002	0.008 ± 0.002	0.015 ± 0.008	0.014 ± 0.006	0.006 ± 0.002	0.004 ± 0.002	0.006 ± 0.002	0.008 ± 0.002	0.010 ± 0.003

Table S1. Hematological toxicities of free SHAL SH7129, conjugated SHAL, free Dox, and different Dox nanoformulations in healthy CD1 mice (female, 10 weeks old). The drug doses were: 10 mg/kg of Dox (either free or encapsulated Dox), 15 μg/kg of free or conjugated Dox, 15 μg/kg SH7129 or conjugated SHAL. Full blood was preserved 48 h after i.v. administration of different formulations for hematological study. (N.B., RBC = red blood cell count; HGB = hemoglobin count; MCV = mean corpuscular volume; MCH = hemoglobin amount per red blood cell; MCHC = mean corpuscular hemoglobin concentration; RET = reticulocytes count; PLT = platelet count; PDW = platelet distribution width; MPV = mean platelet volume; WBC = white blood cell count; NEUT = neutrophils count; LYMPH = lymphocytes count; MONO = mononucleosis count; EO = eosinophilia count; BASO = basophils count. n = 5 per group. * denotes abnormal.)

	Time in days required for tumor to grow to 1,000 cm^3 or death	Absolute growth delay (A.G.D.), day(s) [a]	Normalized growth delay (N.G.D.), days [b]	Enhancement factors (E.F.) (change in tumor sensitivity to XRT, %)[c]
PBS (no treatment)	38.7 ± 2.1			
Free SHAL	35.3 ± 2.3	N/A		
SHAL NPs	35.3 ± 2.6	N/A		
Free Dox	41.7 ± 2.1	3.0 ± 2.1		
Non-targeted Dox NPs	35.9 ± 3.0	N/A		
SHAL-functionalized Dox NPs	45.3 ± 1.8	6.5 ± 1.8		
Free SHAL + free Dox	38.6 ± 1.1	N/A		
SHAL NPs + non-targeted Dox NPs	39.5 ± 2.4	0.8 ± 2.4		
PBS + XRT	56.7 ± 1.3	18.0 ± 1.3		
Free SHAL + XRT	57.7 ± 4.0	19.0 ± 4.0	N/A	N/A
SHAL NPs + XRT	64.1 ± 2.3	25.4 ± 2.3	4.4 ± 2.3	N/A
Free Dox + XRT	74.3 ± 0.8	35.6 ± 0.8	14.5 ± 0.8	N/A
Non-targeted Dox NPs + XRT	50.5 ± 0.8	11.8 ± 0.8	N/A	N/A
SHAL-functionalized Dox NPs + XRT	> 80	> 41.3	> 20.3	> 1.13 (+ 13 %)
Free SHAL + free Dox + XRT	72.2 ± 0.9	33.5 ± 0.9	12.5 ± 0.9	N/A
SHAL NPs + non-targeted Dox NPs + XRT	71.4 ± 1.9	32.7 ± 1.9	11.7 ± 1.9	N/A

Table S2. Table summarizing the absolute growth delay, normalized growth delay and enhancement factor (E.F.) of Daudi-xenograft tumor bearing mice after receiving different chemo-immunotherapy and concurrent CIRT treatment. [[a] Absolute growth delay (A.G.D.) caused by Dox and/or SHAL (co)treatment with/without concurrent XRT is defined as the time in day(s) tumors required to reach 1,000 mm^3 post-inoculation minus the time in days untreated tumors required to grow to 1,000 mm^3. [b] Normalized growth delay (N.G.D.) is defined as time in days for tumors to reach 1,000 mm^3 post-inoculation in mice treated by free/encapsulated Dox with/without free/conjugated SHAL plus radiation minus the time in days for tumors to reach 1,000 mm^3 post-inoculation in mice only received chemotherapy. [c] Enhancement factors (E.F.): obtained by dividing normalized tumor growth delay in mice treated with different chemotherapy plus radiation by the absolute growth delay in mice treat with radiation only. N/A denotes no enhancement (i.e., E.F. < 1).]

	Time in days required for tumor to grow to 1,000 cm^3 or death	Absolute growth delay (A.G.D.), day(s) [a]	Normalized growth delay (N.G.D.), days [b]	Enhancement factors (E.F.) (change in tumor sensitivity to XRT, %)[c]
PBS (no treatment)	34.3 ± 2.3			
Free SHAL	36.9 ± 2.8	2.5 ± 2.8		
SHAL NPs	42.3 ± 2.5	8.0 ± 2.5		
Free Dox	42.3 ± 3.6	8.0 ± 3.6		
Non-targeted Dox NPs	39.3 ± 3.2	5.0 ± 3.2		
SHAL-functionalized Dox NPs	51.3 ± 4.9	17.0 ± 4.9		
Free SHAL + free Dox	35.3 ± 5.4	1.0 ± 5.4		
SHAL NPs + non-targeted Dox NPs	41.9 ± 3.6	7.5 ± 3.6		
PBS + XRT	47.5 ± 3.2	13.2 ± 3.2		
Free SHAL + XRT	41.8 ± 5.0	7.5 ± 5.0	-5.7 ± 5.0	N/A
SHAL NPs + XRT	48.7 ± 2.9	14.4 ± 2.9	1.2 ± 2.9	N/A
Free Dox + XRT	46.5 ± 1.6	17.0 ± 1.6	3.8 ± 1.6	N/A
Non-targeted Dox NPs + XRT	50.5 ± 2.1	16.2 ± 2.1	3.0 ± 0.6	N/A
SHAL-functionalized Dox NPs + XRT	> 80	> 16.2	> 32.5	> 2.46 (+ 146 %)
Free SHAL + free Dox + XRT	41.6 ± 8.9	13.7 ± 8.9	0.5 ± 8.9	N/A
SHAL NPs + non-targeted Dox NPs + XRT	40.0 ± 3.0	5.7 ± 3.0	- 3.5 ± 3.0	N/A

Table S3. Table summarize the absolute growth delay, normalized growth delay and enhancement factor (E.F.) of Raji-xenograft tumor bearing mice after receiving different chemo-immunotherapy and concurrent CIRT treatment. [[a] Absolute growth delay (A.G.D.) caused by Dox and/or SHAL (co)treatment with/without concurrent XRT is defined as the time in day(s) tumors required to reach 1,000 mm^3 post-inoculation minus the time in days untreated tumors required to grow to 1,000 mm^3. [b] Normalized growth delay (N.G.D.) is defined as time in days for tumors to reach 1,000 mm^3 post-inoculation in mice treated by free/encapsulated Dox with/without free/conjugated SHAL plus radiation minus the time in days for tumors to reach 1,000 mm^3 post-inoculation in mice only received chemotherapy. [c] Enhancement factors (E.F.): obtained by dividing normalized tumor growth delay in mice treated with different chemotherapy plus radiation by the absolute growth delay in mice treat with radiation only. N/A denotes no enhancement (i.e., E.F. < 1).]